IAC-08-C1.5.3

EXTENSION OF THE PROXIMITY-QUOTIENT CONTROL LAW FOR LOW-THRUST PROPULSION

CHRISTIE ALISA MADDOCK
Space Advanced Research Team, Dept. of Aerospace Engineering
University of Glasgow, United Kingdom G12 8QQ
email: c.maddock@aero.gla.ac.uk

MASSIMILIANO VASILE
Space Advanced Research Team, Dept. of Aerospace Engineering
University of Glasgow, United Kingdom G12 8QQ
email: m.vasile@aero.gla.ac.uk

Abstract In this paper, the proximity quotient control law, first developed by Petropoulos, is extended to account for both third body effects and solar radiation pressure based on the mission requirements for a hypothetical NEO deflection mission to the asteroid Apophis using a solar sublimation deflection technique. The perturbing effect of solar radiation pressure becomes relevant when dealing with large optics in space. Equations for the disturbing acceleration are derived for the perturbations, then analytically incorporated into the equations determining the rate-of-change in time of the orbital elements, and tested using a Earth-asteroid transfer. Another specific variant of the control law is developed for the orbital maintenance of the spacecraft formation in the vicinity of the NEO.

1 INTRODUCTION

In general, NEO deflection techniques fall into four broad categories [1]: kinetic impactors, propulsive devices, induced changes to the asteroid surface, and ablation devices. A previous study by the authors compared the various deflection methods in terms of: achieved deviation distance, required warning time, total mass into orbit and the estimated technology readiness level. The solar sublimation technique was found to be among the most effective methods. The idea was initially proposed [2] in 1992 and was compared a year later to other deflection methods by Melosh [3, 4]. The concept envisions a large mirror in space which would reflect sunlight onto the surface of the asteroid, sublimating the material and generating a low, continuous thrust due to the force of the ejected debris.

Further preliminary studies were undertaken to determine the feasibility and requirements of such a mission, and developing an initial design for the mirror assembly and orbits for a swarm of spacecraft. The conceptual mission was expanded by the authors to a formation of multiple spacecraft each equipped with a smaller-diameter mirror and collimating lens, instead of one single large mirror (as was first proposed). The collimating lens removed the stringent requirement of operating in close proximity to the asteroid which made the mirror vulnerable to degradation from debris and required complex control to compensate for the inhomogeneous gravity field of the asteroid. A limit on the range still exists to reduce the pointing errors however it is much greater than previously. The proximity-quotient control law, or Q-law, was initially proposed by Petropoulos [5] to generate first-guess solutions for propellant-optimal, low-thrust transfers between two Keplerian orbits. It is based on a Lyapunov feedback control law and calculates the optimal direction of thrust based on the proximity to the target orbit (i.e. the difference in the static Keplerian parameters) and the current location of the spacecraft on the orbit (i.e. true anomaly). The basic Q-law was developed for the restricted two-body problem, based on Gauss' planetary equations.

In this paper, this Q-law is extended based on two different set of criteria using the same NEO deflection missions as the test case. The first calculates the transfer trajectories following the initial deployment of a formation of spacecraft, into their final formation orbits. The second covers a more complex test case where each spacecraft in the formation is required to constantly adjust their orbits in order to maintain a periodic motion with respect to the asteroid.

The following paper is divided into three sections. The first section describes the background calculations for the test case of a NEO deflection mission, in this case the simulated deflection of the asteroid Apophis due to the *relatively* high potential for a series of resonant impacts starting in 2036. The second section describes the original proximity-quotient control law, plus a series of adaptations that were developed for this particular test case. The last section shows the results of applying to the control law to the two different test cases.

2 DESCRIPTION OF TEST CASES

The following section describes the assumptions and design used for NEO deflection mission using a solar sublimation technique, here used as the test case.

2.1 Spacecraft Mirror Assembly Design

Figure 1 shows the mirror configuration design on-board the spacecraft. The primary mirror is paraboloidic in shape, and focuses the rays onto a collimating lens (or system of lenses). The collimated beam is then directed by a smaller flat mirror onto the desired location on the asteroid surface. Due to the large required surface area of the primary mirror, e.g. diameter between 10–30 m, the control law must accommodate the perturbations caused by the solar radiation pressure (SRP).

2.2 Formation Orbit Design

The spacecraft have to maintain their relative position with respect to the asteroid in order to keep the required power density on the same spot of the surface of the asteroid. Therefore, the formation orbits have to be periodic and in close proximity with low excursion in the relative distance from the asteroid. On the other hand the spacecraft should avoid, as much as possible, to fly in the irregular regions of the gravity field of the asteroid. In addition, should also avoid any impingement with the

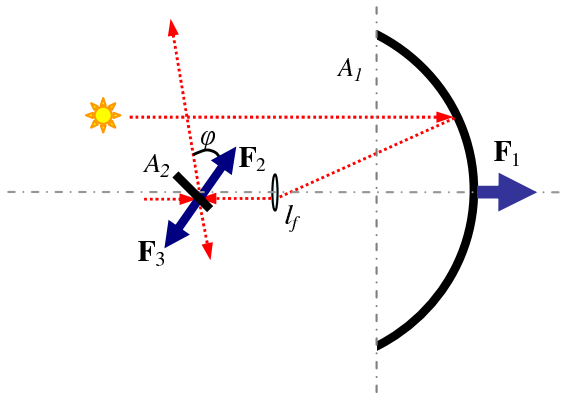

Figure 1: Configuration for mirror assembly: fixed paraboloidic mirror with collimating lens and secondary directional mirror to steer the beam.

plume of debris and gas coming from the sublimation of the surface material.

In order to design the desired formation orbits, we start by considering the linearized relative equations of motion [6],

$$x = \frac{r}{a}\delta a - a\cos f\,\delta e + \frac{ae\sin f}{\eta}\delta M \tag{1a}$$

$$y = \frac{r\sin f\,(2+e\cos f)}{\eta^2}\delta e + r\cos i\delta\Omega + r\delta\omega + \frac{r\,(1+e\cos f)^2}{eta^3}\delta M \tag{1b}$$

$$z = r\sin\theta\delta i - r\cos\theta\sin i\delta\Omega \tag{1c}$$

$$\dot{x} = \frac{\dot{r}}{a}\delta a - a\dot{f}\sin f\,\delta e + \frac{ae\dot{f}\cos f}{\eta^3}\delta M \tag{1d}$$

$$\dot{y} = \frac{(2+e\cos f)\left(\dot{r}\sin f + r\dot{f}\cos f\right) - re\dot{f}\sin^2 f}{\eta^2}\delta e + \dot{r}\cos i\delta\Omega + \dot{r}\delta\omega + \frac{p}{\eta^3 r^2}\left(\dot{r}p - r^2 ef\sin f\right)\delta M \tag{1e}$$

$$\dot{z} = \left(\dot{r}\sin\theta + r\dot{f}\cos\theta\right)\delta i - \sin i\left(\cos\theta - r\dot{f}\sin\theta\right)\delta\Omega \tag{1f}$$

where

$$\dot{r} = re\dot{f}\sin f \qquad \dot{f} = \frac{h}{r^2} \qquad \eta = \sqrt{1-e^2}$$

which use the orbital element differences between a chief orbit (which can be virtual, and is located at the origin of the Hill reference frame) and a

spacecraft in the formation. This is a first approximation of the motion of the spacecraft that does not take into account the gravity field of the asteroid and the solar pressure but it is useful to identify some orbit geometries that answer to our requirements.

The orbital dynamics for the formation are relative to two rotating Hill reference frames, one centered on the asteroid $\mathcal{A}$, and the other centered on the spacecraft $\mathcal{S}$, both in the local radial x, transversal y and normal z directions (see Fig. 2).

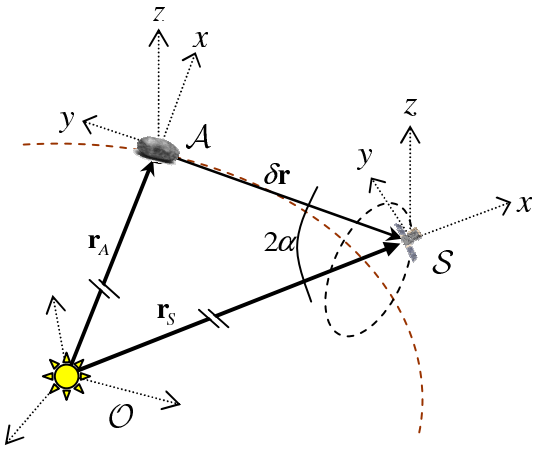

Figure 2: Definition of relative reference frames: $\mathcal{A}$ which is centered on the asteroid, and $\mathcal{S}$ which is centered on the spacecraft. Both are measured in radial x, transversal y and normal z directions.

The formation orbit can be thought of as an orbit around the Sun with a small offset in the initial position $\delta\mathbf{r}_0$ and velocity $\delta\mathbf{v}_0$. This offset can also be expressed as the difference between the orbital parameters of the chief (e.g. Apophis) and the formation. As long as there is no difference in semi-major axes, the two orbits will remain periodic.

$$\delta\mathbf{k} = \mathbf{k}_s - \mathbf{k}_A = [\delta a \;\; \delta e \;\; \delta i \;\; \delta\Omega \;\; \delta\omega \;\; \delta M] \qquad (2)$$

As the mean anomaly is a function of the semi-major axis, the difference in mean anomaly will remain constant through out the orbit so long as $\delta a = 0$.

If the optimal thrust direction that maximizes the deviation is along the unperturbed velocity vector of the asteroid [7], then the exhaust gases will flow along the y-axis of the local Hill reference frame. Therefore, the size of the formation orbits projected in the x-z plane should be maximal. All the requirements on the formation orbits can be formulated in mathematical terms as a multi-objective optimization problem,

$$\min_{\delta\mathbf{k}\in D} \min_{f} J_1 = \delta r \qquad (3)$$

$$\min_{\delta\mathbf{k}\in D} \min_{f} J_2 = -\sqrt{x^2 + z^2} \qquad (4)$$

subject to the constraint

$$C_{ineq} = \min_{f} \left(\delta r(f) - r_{\text{LIM}}\right) > 0 \qquad (5)$$

where r_{LIM} is a minimum-radius sphere imposed to avoid non-linearities in the asteroid gravity field [8], and D is the search space for the solution vector $\delta\mathbf{k}$.

The problem in Eqs. (3)–(5) was solved with a hybrid stochastic-deterministic approach based on a multiagent search technique combined with a decomposition of the search space. For a more detailed description of the optimization algorithms used and the application to formation orbit design, refer to see [9, 10]. Figure 3 shows the resulting set of Pareto-optimal solutions, nicknamed 'funnel' orbits due to their resemblance.

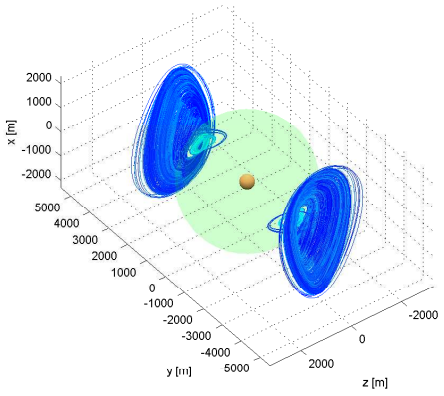

Figure 3: Set of Pareto-optimal solutions for the multi-objective optimization given in (3) to determine possible formation orbits based on given mission requirements (here $r_{\text{LIM}} = 2.3$ km).

The asteroid under test is Apophis 99942 (MN4). The ephemeris and relevant physical characteristics were taken from the NASA Small Bodies database [11].

Two representative formation orbits were chosen out of the Pareto-optimal set to test the control laws. The values for the initial $\delta\mathbf{k}$ are given in Table 1 and Fig. 4. The initial time was set to 5 years prior to the estimated date of impact of Apophis on 13 April 2036. Note, this is the start of the thrusting maneuver, not the launch date from Earth.

Table 1: Optimized initial conditions for formation orbit test cases at $t_0 = 11429.75$ MJD2000.

Parameter		*Value*	
J_1	(m)	88.8845	2463.6755
J_2	(m)	-241.1802	-892.0682
δa	(km)	0	0
δe		6.9071E-12	-5.7472E-13
δi	(rad)	-1.7903E-09	-1.2645E-08
$\delta\Omega$	(rad)	-2.3827E-08	-5.0000E-08
$\delta\omega$	(rad)	3.1574E-08	3.3794E-08
δM	(rad)	8.9855E-09	3.7997E-08

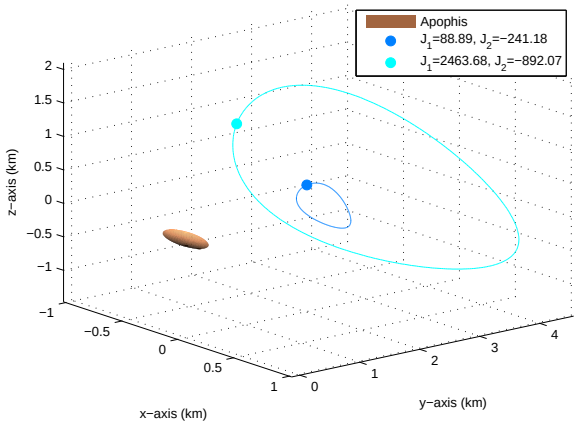

Figure 4: Two formation orbits used as test cases.

3 CONTROL LAW EXTENSIONS

3.1 Q-law Control

The proximity-quotient control law, or Q-law, was first proposed by Petropoulos [5] in 2003 to generate first guess approximations for propellant-optimal, low-thrust transfers between two Keplerian orbits. It is based on a Lyapunov feedback control law and calculates the optimal direction of thrust $[\alpha, \beta]$ based on the proximity to the target orbit (i.e. the difference in the static Keplerian parameters) and the current location of the spacecraft on the orbit (i.e. true anomaly f). The basic Q-law was developed for the restricted two-body problem, based on Gauss' planetary equations, given below [12].

$$\frac{da}{dt} = \frac{2a^2 e \sin f}{h} u_x + \frac{2a^2 p}{hr} u_y \tag{6a}$$

$$\frac{de}{dt} = \frac{p \sin f}{h} u_x + \frac{(p+r)\cos f + re}{h} u_y \tag{6b}$$

$$\frac{di}{dt} = \frac{r \cos\theta}{h} u_z \tag{6c}$$

$$\frac{d\Omega}{dt} = \frac{r \sin\theta}{h \sin i} u_z \tag{6d}$$

$$\frac{d\omega}{dt} = -\frac{p \cos f}{he} u_x + \frac{(p+r)\sin f}{he} u_y - \frac{r \sin\theta \cos i}{h \sin i} u_z \tag{6e}$$

where $\mathbf{u}$ represents the disturbing acceleration,

$$\mathbf{u} = \begin{bmatrix} u_x \\ u_y \\ u_z \end{bmatrix} = \begin{bmatrix} u \sin\alpha \cos\beta \\ u \cos\alpha \cos\beta \\ u \sin\beta \end{bmatrix} \tag{7}$$

in the radial x, transversal y and normal z directions where $\mathbf{k}$ is the set of Keplerian orbit elements, $\theta = f + \omega$ is the true latitude, $p = a(1-e^2)$ is the semi-latus rectum, μ is the gravitation constant of the central body, n is the mean motion and h is the angular orbital momentum.

Analytical equations were found for the direction of thrust $[\alpha_{xx}, \beta_{xx}]$ and true anomaly f_{xx} that maximized the rate of change of each orbital element, $\dot{\mathbf{k}}_{xx}$. Since the Q-law was designed for transfer trajectories between two Keplerian orbits (and not "point-to-point" transfers), the rate of change of the true (or mean) anomaly was ignored.

These maximized rates of change were summed, along with the desired difference in the time-invariant Keplerian parameters to generate the proximity-quotient equation [5].

$$Q = \sum_{j=1}^{5} W_{k_j} \left(\frac{k_{i,j} - k_{T,j}}{\dot{k}_{xx,j}} \right)^2 \tag{8}$$

where W_k are a set of weights between [0 1], and i and T are the initial and target states respectively. The Lyapunov function is simply the rate of change of Q with time. The partial derivatives of Q for each of the first five elements in $\mathbf{k}$ can be solved analytically. The optimal thrust angles at any point in time can be determined by finding the global minimum of dQ/dt.

$$\dot{Q} = \frac{\partial Q}{\partial \mathbf{k}} \frac{d\mathbf{k}}{dt} \tag{9}$$

where $d\mathbf{k}/dt$ are given by (6).

A number of refinements were added later by Petropolous [13]. In this analysis, a measure of the absolute efficiency of the control was used to turn off the thrust when the efficiency of the rates-of-change of the desired orbital elements is below 50%.

$$\eta_{abs} = \frac{\min\limits_{\alpha,\beta}(\dot{Q})}{\dot{Q}_{nx}} \tag{10}$$

where the measure of the best performance (at the maximum rates of change) is given by,

$$\dot{Q}_{nx} = \sum_{j=1}^{5} \frac{\partial Q}{\partial k_j} \dot{k}_{xx,j} \tag{11}$$

3.2 Perturbations

Two additional perturbations need to be accounted for in the control: the solar radiation pressure due to the size of the mirrors, and the effects of the gravity field of the asteroid.

The general equation for the magnitude of acceleration due to solar radiation pressure is,

$$\ddot{r}_{\text{SRP}} = \frac{2S_0}{c}\frac{\eta_{\mathit{eff}} A}{m_s}\left(\frac{r_{\text{AU}}}{r_s}\right)^2 \cos^2\phi \cdot \hat{\mathbf{n}} \tag{12}$$

where S_0 is the solar flux density at 1 AU (1367 W/m^2), c is the speed of light, η_{eff} is the efficiency, A is the surface area, m_s is the mass of the spacecraft, r_s is the distance between the Sun and the spacecraft, and lastly ϕ is the angle of reflection. The SRP always acts in the direction normal $\hat{\mathbf{n}}$ to the mirror surface.

As the primary mirror is always in line with the Sun, the force $\mathbf{F}_1$ is in the radial direction in the spacecraft-centric reference frame $\mathcal{S}$. For the secondary mirror, two forces are accounted for: $\mathbf{F}_2$, the reflected SRP from the primary mirror, and $\mathbf{F}_3$, the force due to the SRP from the Sun acting on the 'back' of the mirror (see Fig. 1).

$$\mathbf{F}_1 \rightarrow \mathbf{s}_p = \frac{2P_0}{m_s r_s^2}\eta_{\mathit{eff}} A_p\, \hat{\mathbf{x}} \tag{13}$$

$$\mathbf{F}_2 + \mathbf{F}_3 \rightarrow \mathbf{s}_d = \frac{2P_0}{m_s r_s^2}\eta_{\mathit{eff}} \cos^2\phi\,(A_d - \eta A_p)\cdot \frac{\mathbf{n}_d}{\|\mathbf{n}_d\|} \tag{14}$$

where $P_0 = r_{\text{AU}}^2 S_0/c$. In the following we will take into account only the contribution of the forces due to the orbital dynamics but it should be noted that the combination of $\mathbf{F}_2$ and $\mathbf{F}_3$ will induce a consistent torque on the mirror assembly.

The unit vector for the direction of the solar pressure on the direction mirror $\hat{\mathbf{n}}_d$ is derived in terms of Keplerian orbital elements relative to the Hill frame centered on the spacecraft.

$$\mathbf{n}_d = \begin{bmatrix} -\sqrt{\frac{\Gamma}{2\,\delta r}}\,(r_s + r_{\text{A}}\varrho\cos\theta + r_{\text{A}}\zeta\sin\theta) \\ r_{\text{A}}\big(\cos i\cos(\delta\theta\text{–}\theta)\cos\theta\sin\delta\Omega \\ \quad +\xi\cos\theta\sin(\delta\theta\text{–}\theta) - \varrho\sin\theta\big) \\ r_{\text{A}}\big(\cos(\delta\theta\text{–}\theta)\sin\delta\Omega\sin i + \varpi\sin(\delta\theta\text{–}\theta)\big) \\ \quad \big(\sqrt{\frac{2\Gamma}{\delta r}} + r_s(r_s + r_{\text{A}}\varrho\cos\theta + r_{\text{A}}\zeta\sin\theta)\big) \end{bmatrix} \tag{15}$$

where

$$\varpi = \cos i\sin(\delta i\text{–}i) + \cos\delta\Omega\cos(\delta i\text{–}i)\sin i \tag{16a}$$

$$\xi = \cos\delta\Omega\cos(\delta i\text{–}i)\cos i - \sin(\delta i\text{–}i)\sin i \tag{16b}$$

$$\varrho = -\cos\delta\Omega\cos(\delta\theta\text{–}\theta) + \cos(\delta i\text{–}i)\sin\delta\Omega\sin(\delta\theta\text{–}\theta) \tag{16c}$$

$$\zeta = \cos i\cos(\delta\theta\text{–}\theta)\sin\delta\Omega + \xi\sin(\delta\theta\text{–}\theta) \tag{16d}$$

$$\Gamma = \delta r + r_s - r_{\text{A}}\big(\cos\delta\Omega\cos(\delta\theta\text{–}\theta)\cos\theta + \cos(\delta i\text{–}i)\cos\theta\sin\delta\Omega\sin(\delta\theta\text{–}\theta) + \zeta\sin\theta\big) \tag{16e}$$

Similarly, the vector from the spacecraft to the asteroid, $\delta\mathbf{r}$, can be expressed in the spacecraft-centered Hill reference frame $\mathcal{S}$ by means of geometry.

$$\delta\mathbf{r} = -\mathbf{r}_s - \mathbf{r}_{\text{A}}\begin{bmatrix} \varrho\cos\theta + \zeta\sin\theta \\ -\zeta\cos\theta + \varrho\sin\theta \\ -\cos(\delta\theta\text{–}\theta)\sin\delta\Omega\sin i \\ +\varpi\sin(\delta\theta\text{–}\theta) \end{bmatrix} \tag{17}$$

Note that it is also possible to use the linearized equations of motion in (1) as long as $\delta\mathbf{r} \ll \mathbf{r}_s$, however since the computation time is the same, the more exact equations were used.

Lastly, the angle of reflection is re-derived in terms of the orbital elements,

$$\cos^2\alpha = \frac{r_{\text{A}}^2}{2\delta r|\Gamma|}\big(\cos(\delta\theta\text{–}\theta)\sin\delta\Omega\sin i + \varpi\sin(\delta\theta\text{–}\theta)\big)^2 \tag{18}$$

Since the effects of the asteroid's gravity field outside the imposed limiting sphere are relatively linear [8], and much less compared to those due the solar radiation pressure, the asteroid is treated, as a first approximation, as a point mass with μ_A = 1.8016E-9 km^3/s^2 (the mass is taken as 27E9 kg). The Gauss equations in (6) can be re-expressed using a modified disturbing acceleration

vector accounting for the solar radiation pressure, and the third body effects [14].

$$\mathbf{u}_{pert} = (\mathbf{s}_p + \mathbf{s}_d) + \mu_{\text{A}} \left(\frac{\delta \mathbf{r}}{\delta r^3} - \frac{\mathbf{r}_s}{r_s^3} \right) \tag{19}$$

where $\mathbf{s}_p$, $\mathbf{s}_d$ are the disturbing acceleration vectors due to SRP defined in (13) and (14) respectively.

3.3 Orbital Maintenance

For the maintenance of the formation orbit, a number of issues that arose when using the Q-law: the first was due to the high degree of accuracy need to maintain the funnel orbits. The difference in Keplerian between the NEO and the spacecraft are on the order of 10^{-7}, and need to remain constant even as the NEO deviates. This resulted in a lot of 'chatter' (over-shooting) around the target orbital elements, due to strong dependence on the time step δt and the magnitude of the control (which employed on-off shooting). Even at very small time steps, the magnitude of the over-shooting was too large for the system requirements. In addition, the effects of the individual perturbations are relatively large (shown in Figs. 5 and 6) and need to be compensated for on a continuous basis.

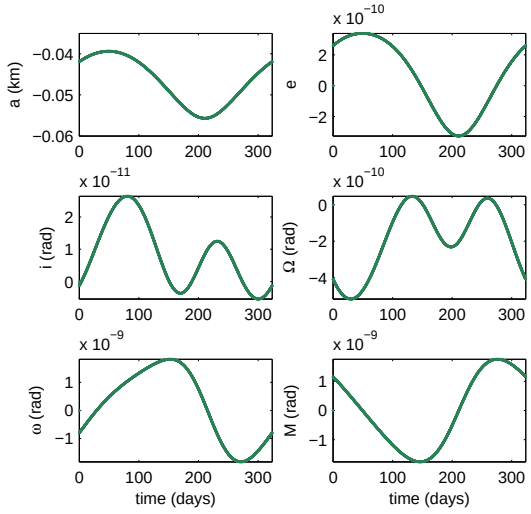

Figure 5: Effects of third-body perturbations on an un-controlled formation orbit.

Therefore a variant of the control law was developed to account for these limitations.

3.3.1 Mean anomaly

Due to the nature of the formation orbits, the difference in mean anomaly must also be controlled.

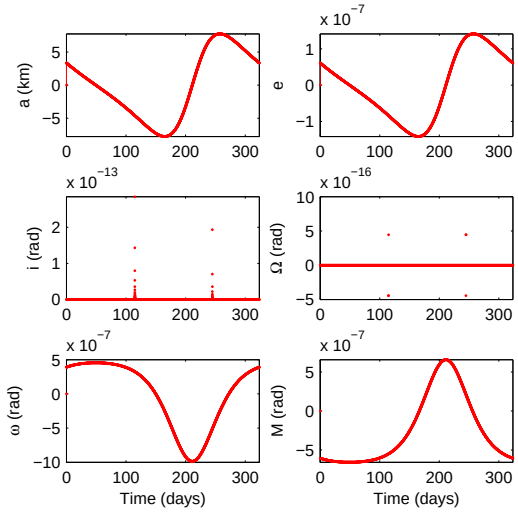

Figure 6: Effects of solar radiation pressure on an uncontrolled formation orbit with a 20 m primary mirror, and 1 m diameter secondary mirror.

The actual Gauss equation for dM/dt also includes a term for the mean motion n to account for the rotation around the Sun. In this case however, we do not want the control to compensate for the nominal motion of the orbit, just those induced by the perturbations and deviation of the asteroid. The mean motion is added to M^* after each iteration of the simulation control loop, where $M_i = M^* + n_s \delta t$ (since the nominal rate of the change of the mean anomaly is linear).

$$\frac{dM^*}{dt} = \frac{p\cos f - 2re}{e\sqrt{a\mu}} u_x - \frac{(p+r)\sin f}{e\sqrt{a\mu}} u_y \tag{20}$$

3.3.2 Least-Squares Approach

In addition to accounting for the above perturbations within the control law, a number of changes were introduced to further refine the algorithm to the specific test case. The first was to switch from minimizing only the thrust angles $[\alpha, \beta]$, to directly minimizing the components $[u_x, u_y, u_z]$ which has the benefit of finding the optimal magnitude for the thrust, as well as the required angles. The new control function is given by,

$$Q^* = \sum_{j=1}^{6} \left(W_{k_j} (\Delta k_{i,j} - \Delta k_{T,j}) \right)^2 \tag{21}$$

where $\Delta \mathbf{k}_T = (\mathbf{k}_i - \mathbf{k}_T)$ is the desired variation of the orbital parameters. The function Q^* is then minimized with respect to the applied control $\mathbf{u}_c$.

Inherently, if the desired change in the j^{th} element $(k_{i,j} - k_{T,j})$ is negative, than the rate of change $\dot{\mathbf{k}}_j$ is positive, and vice versa. As such, the control equation will always have a single minimum, therefore we can directly minimize Q^*, instead of minimizing the time derivative.

If we consider that over very small time steps, we can assume as first approximation that the orbital parameters in the Gauss equations are constant,

$$\Delta k_{i,j} \approx \frac{d\mathbf{k}}{dt}\delta t \tag{22}$$

than the solution control vector $\mathbf{u}_c$ can be found by using an ordinary least squares fitting to the linear systems of equations $\mathbf{A} \cdot \mathbf{u}_c = \mathbf{b}$. Here, the matrix $\mathbf{A}$ is set equal to the Gauss equations in (6) as a function of the applied control $\mathbf{u}_c$ only (i.e. no perturbations). The vector $\mathbf{b}$ is given by,

$$\mathbf{b} = \frac{\mathbf{k}_i - \mathbf{k}_T}{\delta t} - \mathbf{A}\mathbf{u}_{pert} \tag{23}$$

where $\mathbf{u}_{pert}$ is given in (19). Again, this is equivalent to minimizing the quadratic function $\Sigma(\Delta\mathbf{k}_{i,j} - \Delta\mathbf{k}_{T,j})^2$ where $\Delta k_{i,j}$ is the change of the j^{th} orbital element over time δt calculated using the Gauss equations, and $\Delta k_{T,j}$ is the desired change. The weights are used to scale individual parameters to increase (or decrease) their sensitivity.

3.3.3 Integration Approach

An integration approach can also be used with the same control function Q^* in (21) which numerically integrates the Gauss equations to determine $\Delta k_{i,j}$.

$$\Delta k_{i,j} = \int_0^{\delta t} \frac{dk_j}{dt} dt \tag{24}$$

The least-squares approach provides a computationally faster solution (for the same time step) but is less accurate, especially over larger time steps.

4 SIMULATION RESULTS

4.1 Earth-Formation Transfer

The true anomaly at the departure from the Earth is free, whereas the one at the termination point is fixed. As such, the Q-law was run 'backwards' from the specific initial state vector required by the formation orbit, at a specified t_0 (here set to 5 years prior to the first potential impact on 13 April 2036), to a parking orbit around Earth.

Three different simulations were run. Figures 7–8 show the baseline comparison using only the gravitational effects from the Sun ($\mathbf{u} = \mathbf{u}_c$). Figures 9–10 show the effect of using the same Gauss equations with no perturbations within the control law, but accounting for the additional perturbations when propagating the orbit. Lastly, Figures 11–12 show the effects of accounting for the perturbations within the control law. The time step δt was set to 1 h (3600 s). For the transfer, only the in-plane case was considered (i.e. $\beta \Rightarrow 0$). The control is therefore correcting only a, e and ω.

The 'on-off' scheme for the control can be seen in the plots of the control components, where the thrust switches off when the efficiency of the change in the desired Keplerian parameters drops below 50%. While the prolongs the transfer time, it provides a more efficient transfer.

4.2 Formation Orbit Maintenance

The algorithm used to simulate the required maintenance of the formation orbit for the deflection mission is given below.

Step 1 Initialize starting conditions at t_0 for each spacecraft and NEO, $\mathbf{k}_T = \mathbf{k}_i = \mathbf{k}_0$.

Step 2 Determine optimal control vector $\mathbf{u}_c$ solving using either the least-squared method or integration method, given current state $\mathbf{k}_i$, target state $\mathbf{k}_T$, and position of the deviated asteroid $\mathbf{k}_A$.

Step 3 Propagate $\mathbf{r}_s$, $\mathbf{v}_s$ forward by time step δt using Gauss equations with input $(\mathbf{u}_c + \mathbf{u}_{pert})$, and update the current state $\mathbf{k}_i(t + \delta t)$.

Step 4 Propagate asteroid given thrust due to the solar sublimation again by numerically integrating Gauss equations, and update $\mathbf{k}_A(t + \delta t)$. Note: a description for the method for determining the generated thrust can be found in [7].

Step 5 Update target state, $\mathbf{k}_T(t+\delta t) = \mathbf{k}_A(t+\delta t) + \delta\mathbf{k}$.

REPEAT from Step 2.

Figures 13 and 15 show the difference in Keplerian parameters between the current and target states for a small segment of the mission using the least squares control approach. Figures 14 and 16 show the corresponding control in the radial, transverse and normal components. The time step δt was set to 1 s. Two different weights W_k were used: the baseline with all the weights set to 1, and a second set which increases the weight of a and decreases that of e, $\mathbf{W}_k = [10^6, 10^{-6}, 1, 1, 1, 1]$. The result is a finer control, especially around a which has the largest difference. The oscillations in the Keplerian parameters are due to the internal integration steps of the Gauss equations, where

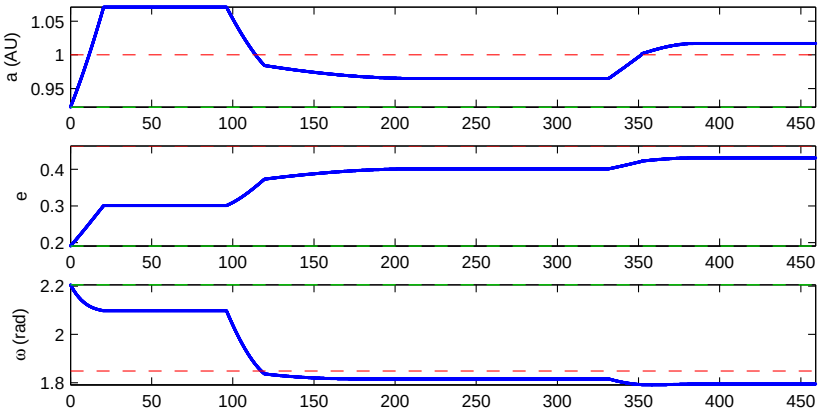

Figure 7: Change of in-plane Keplerian parameters during reverse transfer trajectory from the asteroid to Earth, with no perturbations in either the dynamics nor the control law.

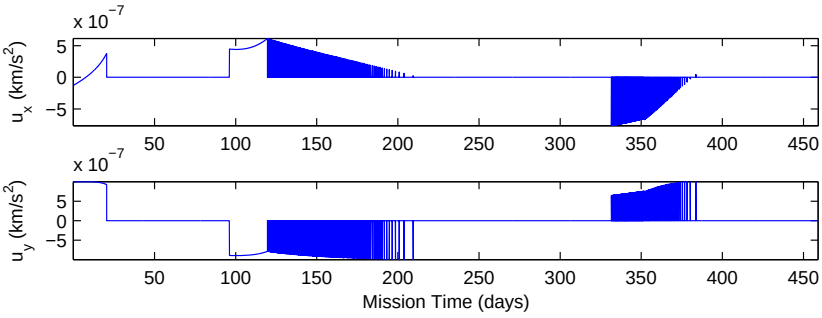

Figure 8: Control components during reverse transfer trajectory from the asteroid to Earth, with no perturbations in either the dynamics nor the control law.

the period of the oscillations is equal to the time step δt.

Figures 15–16 show, by comparison, the same simulation parameters using the integration approach.

5 CONCLUSION

Based on the work done by Petropolous on the proximity-quotient control law, we have created a number of application-specific variants based on a test mission to deflect a Near Earth Object deemed a potentially hazardous to Earth. The control law was modified to account for additional perturbations due to solar radiation pressure on the large mirror surface, and third body effects from the asteroid, relevant during the deflection segment. Two test cases were presented: the first uses an orbit-to-point transfer from the Earth to the initial state vector of the formation orbit near Apophis, and the second is to test the control for the maintenance of the formation orbits countering the solar radiation pressure, third body effects from Apophis and the deviation of the Apophis.

Preliminary results were presented showing promise for the control modifications. Additional work is still needed to fine tune the parameters, such as the weights and time step, and in the case of the transfer trajectory the magnitude of the applied thrust. Properly adjusting these values will decrease the overshooting of the target states.

ACKNOWLEDGMENTS

This research is partially supported by the ESA/Ariadna Study Grant AO/1-5387/07/NL/CB. The authors would like to thank Dr. Leopold Summerer of the ESA Advanced Concepts Team for his support.

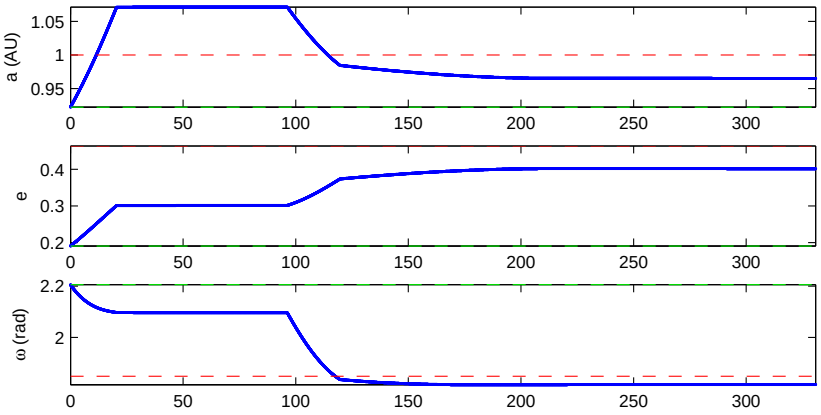

Figure 9: Change of in-plane Keplerian parameters during reverse transfer trajectory from the asteroid to Earth, with perturbations in the dynamics but not in the control law.

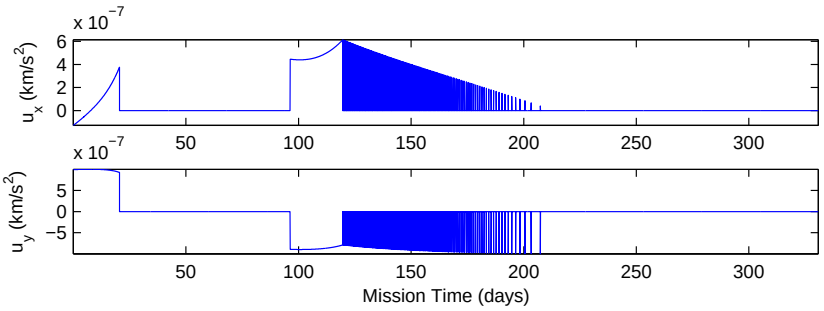

Figure 10: Control components during reverse transfer trajectory from the asteroid to Earth, with perturbations in the dynamics but not in the control law.

REFERENCES

[1] Sanchez Cuartielles, J. P., Colombo, C., Vasile, M., and Radice, G., "Multi-criteria Comparison among Several Mitigation Strategies for Dangerous Near Earth Objects," *Journal of Guidance, Control and Dynamics*, To appear, Accepted 2008.

[2] Lunan, D., "Need we protect Earth from space objects and if so, how?" *Space Policy*, Vol. 8, No. 1, 1992, pp. 90–91.

[3] Melosh, H. J. and Nemchinov, I. V., "Solar asteroid diversion," *Nature*, Vol. 366, No. 366, 1993, pp. 21–22.

[4] Melosh, H. J., Nemchinov, I. V., and Zetzer, Y. I., "Non-nuclear strategies for deflecting comets and asteroids," *Hazard due to comets and asteroids*, edited by T. Gehrels, University of Arizona Press, 1994, pp. 1111–1132.

[5] Petropoulos, A., "Simple control laws for low-thrust orbit transfers," *AIAA/AAS Astrodynamics Specialists' Conference*, AIAA, Montana, U.S.A., August 2003.

[6] Schaub, H. and Junkins, J. L., *Analytical mechanics of space systems*, AIAA Education Series, Virginia, U.S.A., 1st ed., 2003.

[7] Vasile, M. and Colombo, C., "Optimal Impact Strategies for Asteroid Deflection," *Journal of Guidance, Control and Dynamics*, Vol. 31, No. 4, July–August 2008, pp. 858–872.

[8] Sanchez Cuartielles, J. P., Colombo, C., Vasile, M., and Radice, G., "A Multi-criteria Assessment of Deflection Methods for Dangerous NEOs," *American Institute of Physics – New Trends in Astrodynamics and Applications III*, edited by E. Belbruno, Vol. 886, 2007, pp. 317–333.

[9] Vasile, M., *Multi-Objective Memetic Algorithms*, chap. Hybrid Behavioral-Based Multiobjective Space Trajectory Optimization, Studies in Computational Intelligence, Springer, 2008.

[10] Maddock, C. and Vasile, M., "Design of optimal spacecraft-asteorid formations through a hybrid

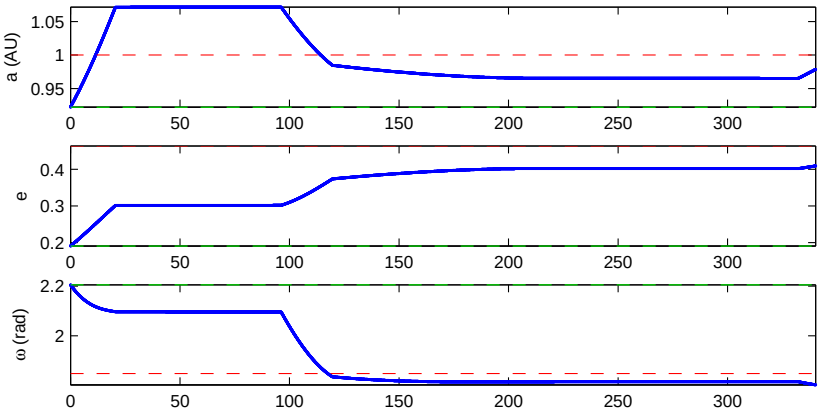

Figure 11: Change of in-plane Keplerian parameters during reverse transfer trajectory from the asteroid to Earth, with perturbations in both the dynamics and control law.

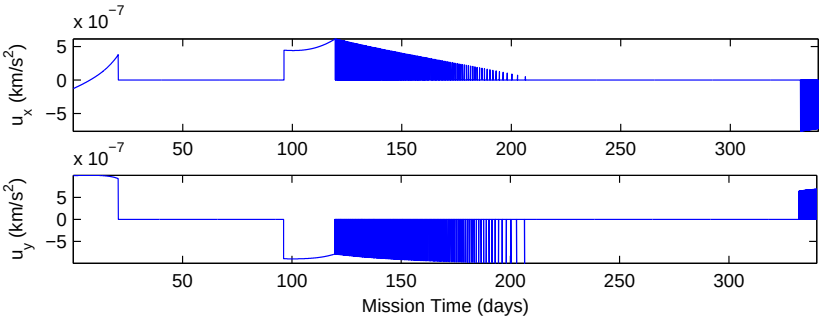

Figure 12: Control components during reverse transfer trajectory from the asteroid to Earth, with perturbations in both the dynamics and control law.

global optimization approach," *Journal of Intelligent Computing and Cybernetics*, Vol. 1, No. 2, 2008, pp. 239–268.

[11] NASA Near Earth Object Program, "99942 Apophis (2004 MN4) Impact Risk," Online Database, http://neo.jpl.nasa.gov/risk/a99942.html, August 2008.

[12] Battin, R. H., *An Introduction to the Mathematics and Methods of Astrodynamics*, AIAA Education Series, revised ed., 1999.

[13] Petropoulos, A., "Refinements to the Q-law for low-thrust orbit transfers," *AIAA/AAS Astrodynamics Specialists' Conference*, AIAA, California, U.S.A., August 2005.

[14] Vallado, D. A., *Fundamentals of Astrodynamics and Applications*, The Space Technology Library, Microcosm Press Kluwer Academic Publishers, 2nd ed., 2004.

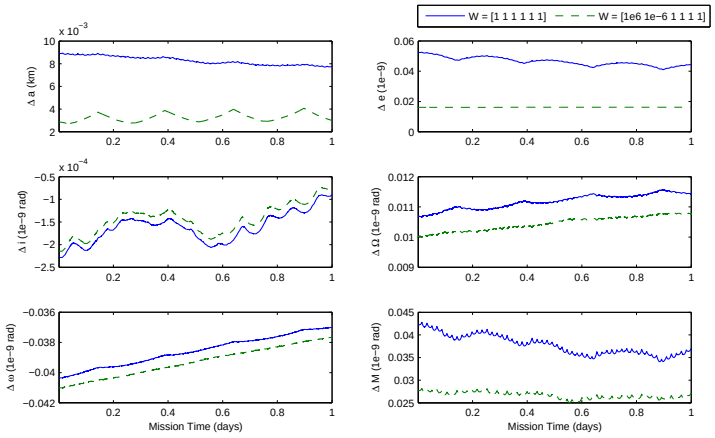

Figure 13: Difference between the current and target states of the formation orbit A ($J_1 = 88.88$, $J_2 = 2463.67$) with least square control, using two different sets of weights $\mathbf{W}_k$ (*Note*: all the values except a are scaled by 10^{-9}).

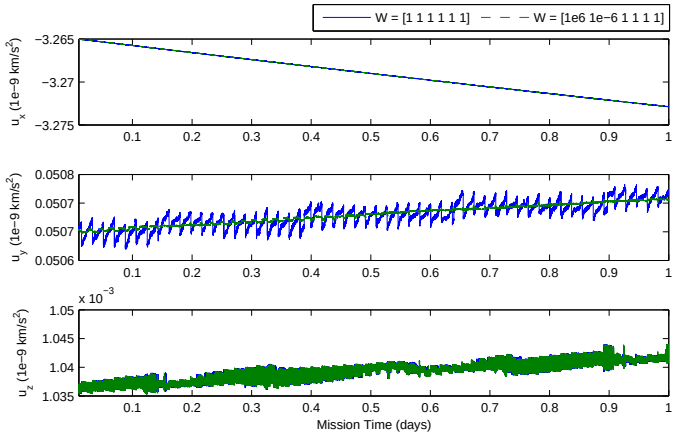

Figure 14: Control components for formation orbit A ($J_1 = 88.88$, $J_2 = 2463.67$) with least square control, using two different sets of weights $\mathbf{W}_k$ (*Note*: all the values are scaled by 10^{-9}).

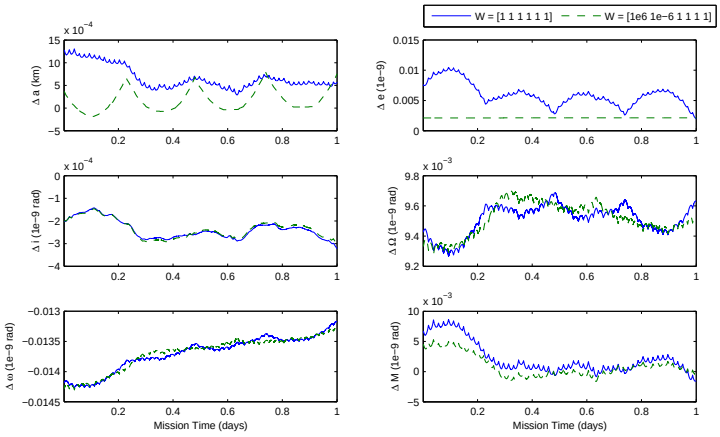

Figure 15: Difference between the current and target states of the formation orbit B ($J_1 = -241.18$, $J_2 = -892.07$) with least squares control, using two different sets of weights $\mathbf{W}_k$ (*Note*: all the values except a are scaled by 10^{-9}).

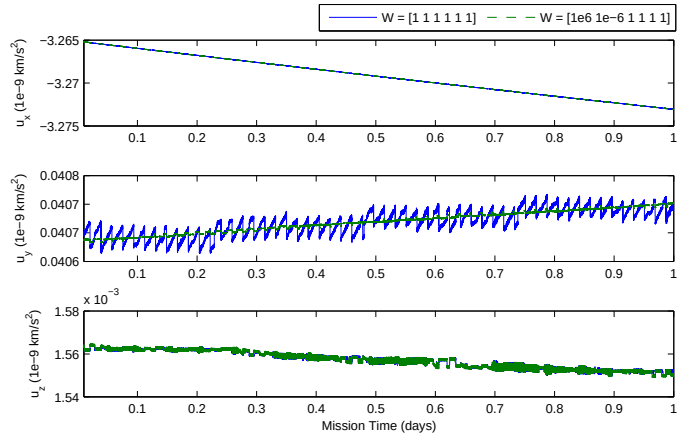

Figure 16: Control components for formation orbit B ($J_1 = -241.18$, $J_2 = -892.07$) with least square control, using two different sets of weights $\mathbf{W}_k$ (*Note*: all the values are scaled by 10^{-9}).

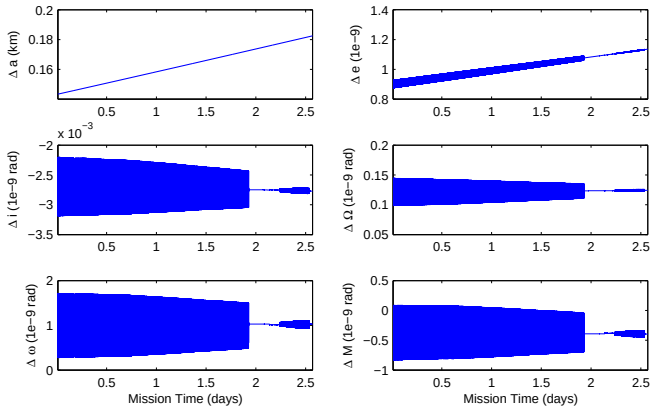

Figure 17: Difference between the current and target states of the formation orbit A ($J_1 = 88.88$, $J_2 = 2463.67$) with integration control (*Note*: all the values except a are scaled by 10^{-9}).

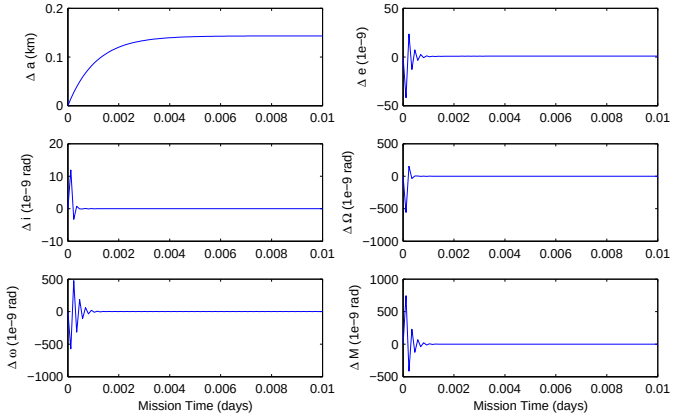

Figure 18: Magnification of Fig. 17, for difference between the current and target states of the formation orbit A ($J_1 = 88.88$, $J_2 = 2463.67$) with integration control (*Note*: all the values except a are scaled by 10^{-9}).

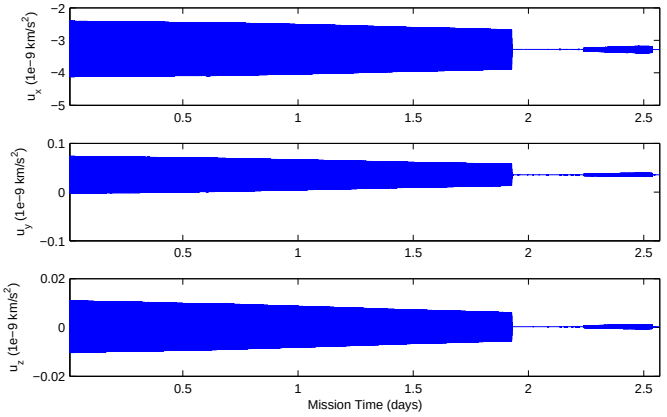

Figure 19: Control components for the formation orbit A ($J_1 = 88.88$, $J_2 = 2463.67$) with integration control (*Note*: all the values are scaled by 10^{-9}).

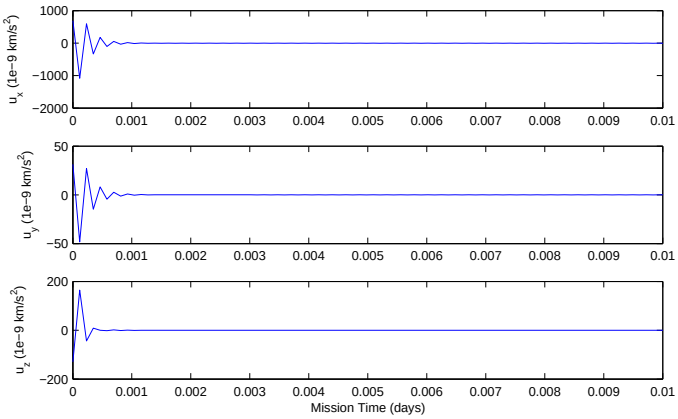

Figure 20: Magnification of Fig. 19, control components for the formation orbit A ($J_1 = 88.88$, $J_2 = 2463.67$) with integration control (*Note*: all the values are scaled by 10^{-9}).

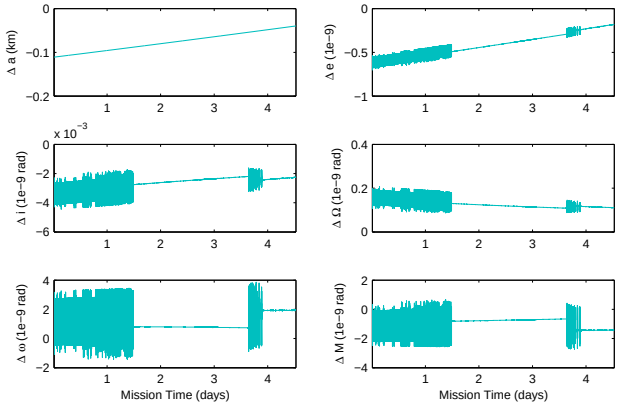

Figure 21: Difference between the current and target states of the formation orbit B ($J_1 = -241.18$, $J_2 = -892.07$) with integration control (*Note*: all the values except a are scaled by 10^{-9}).

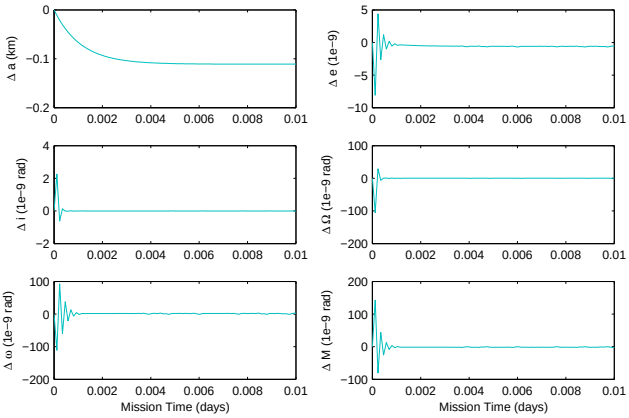

Figure 22: Magnification of Fig. 21, for difference between the current and target states of the formation orbit B ($J_1 = -241.18$, $J_2 = -892.07$) with integration control (*Note*: all the values except a are scaled by 10^{-9}).

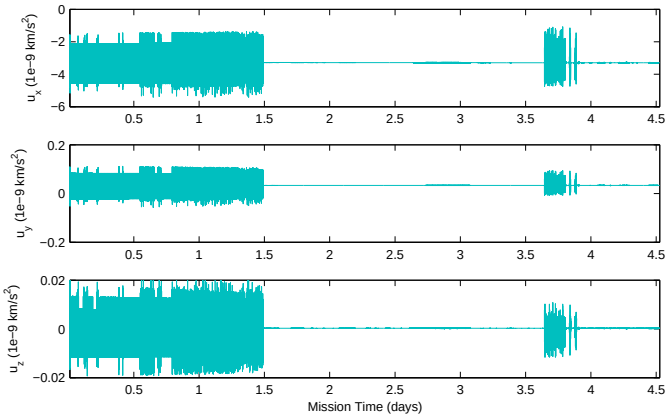

Figure 23: Control components for the formation orbit B ($J_1 = -241.18$, $J_2 = -892.07$) with integration control (*Note*: all the values are scaled by 10^{-9}).

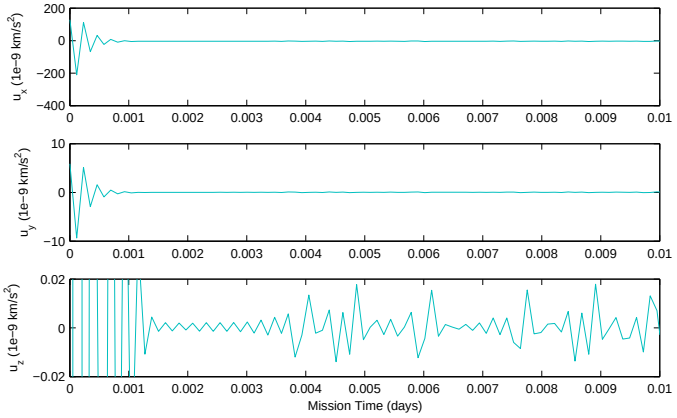

Figure 24: Magnification of Fig. 23, control components for the formation orbit B ($J_1 = -241.18$, $J_2 = -892.07$) with integration control (*Note*: all the values are scaled by 10^{-9}).